EPJ Web of Conferences **113**, 06009 (2016)
DOI: 10.1051/epjconf/201611306009

Contributions of chiral two- and three-nucleon interactions to closed shell nuclei

Yiharn Tzeng[1,a], Shwu-Yun Tsay Tzeng[2,b], and T. T. S. Kuo[3,c]

[1] *Institute of Physics, Academia Sinica, Taipei 11529, Taiwan, ROC*
[2] *Dept. of Electro-Optical Engineering, National Taipei University of Technology, Taipei 10608, Taiwan, ROC*
[3] *Department of Physics, State University New York at Stony Brook, Stony Brook , New York 11794, USA*

Abstract. Using two-nucleon force alone is usually inadequate to interpret nuclear systems' experimental data. We adopt a chiral N^3LO two-nucleon potential V_{2N} with the inclusion of an in-medium three-nucleon (NNN) force $\bar{V}_{3N}$ to calculate binding energies of closed-shell nuclei. The matrix elements of low momentum nucleon-nucleon potential V_{low-k} obtained from integrating the high momentum part of a realistic potentials is inputted in the particle-particle hole-hole ring diagram calculation to study nuclear properties. Nuclear binding energies are accurately reproduced. Without this three-nucleon force, the nuclear binding energy is too weak, as already known. The correction from ring diagrams of order higher than 1 can not be ignored.

The main purpose of this work is to investigate the contributions of a chiral N^3LO two-nucleon potential V_{2N} and an in-medium three-nucleon (3N) force V_{3N}[1] to binding energies of closed shell nuclei, such as ^{16}O, and ^{40}Ca. To achive this aim, we perform the calculation in the framework of a ring diagram expansion[2, 3], as shown in Fig. 1. The particle-particle hole-hole ring diagrams are summed to all orders in this expansion. This method has been applied to several calculations on nuclear matter and neutron star as well as on cold neutron matter at the unitary limit. Applications to finite nuclei[3] have been quite limited. Such ring-diagram calculations for closed-shell nuclei using realistic V_{2N} and V_{3N} have not been carried out. The low momentum V_{low-k} effective interaction matrix elements[4] of V_{2N} and V_{3N} are calculated for the uses in the ring diagram formulism. This V_{low-k} interaction has been successfully applied to finite nuclei in shell model calculations and studies in neutron matter.

The leading contribution to V_{3N} occurs at N^{2}LO in the chiral power counting and is composed of a long-range two-pion exchange component $V_{3N}^{(2\pi)} = \sum_{i\neq j\neq k} \frac{g_A^2}{8f_\pi^4} \frac{\vec{\sigma}_i\cdot\vec{q}_i\,\vec{\sigma}_j\cdot\vec{q}_j}{(\vec{q}_i^{\,2}+m_\pi^2)(\vec{q}_j^{\,2}+m_\pi^2)} F_{ijk}^{\alpha\beta}\tau_i^\alpha\tau_j^\beta$, a medium-range one-pion exchange term $V_{3N}^{(1\pi)} = -\sum_{i\neq j\neq k} \frac{g_A c_D}{8f_\pi^4\Lambda_\chi} \frac{\vec{\sigma}_j\cdot\vec{q}_j}{\vec{q}_j^{\,2}+m_\pi^2}\vec{\sigma}_i\cdot\vec{q}_j\,\vec{\tau}_i\cdot\vec{\tau}_j$, and a pure contact interaction $V_{3N}^{(\mathrm{ct})} = \sum_{i\neq j\neq k} \frac{c_E}{2f_\pi^4\Lambda_\chi}\vec{\tau}_i\cdot\vec{\tau}_j$, where $g_A = 1.29$, $f_\pi = 92.4$ MeV, $\Lambda_\chi = 700$ MeV, $m_\pi = 138.04$ MeV/c^2 is the average pion mass, $\vec{q}_i = \vec{p}_i{}' - \vec{p}_i$ is the difference between the final and initial momentum of nucleon i and $F_{ijk}^{\alpha\beta} = \delta^{\alpha\beta}\left(-4c_1m_\pi^2 + 2c_3\vec{q}_i\cdot\vec{q}_j\right) + c_4\epsilon^{\alpha\beta\gamma}\tau_k^\gamma\vec{\sigma}_k\cdot\left(\vec{q}_i\times\vec{q}_j\right)$. The low-energy constants $c_1 = -0.76\,\mathrm{GeV}^{-1}$, $c_3 = -4.78\,\mathrm{GeV}^{-1}$, and $c_4 = 3.96\,\mathrm{GeV}^{-1}$ appear already in the N^{2}LO two-nucleon

[a] e-mail: phtzengyh@sinica.edu.tw
[b] e-mail: sytsay@mail.ntut.edu.tw
[c] e-mail: kuo@tonic.physics.sunysb.edu

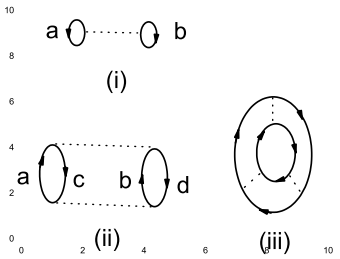

Figure 1. Some lowest order ring diagrams.

potential and are therefore constrained by low-energy NN phase shifts. The low-energy constants c_D and c_E are typically fit to reproduce the properties of light nuclei[5].

We then calculate effective low momentum V_{low-k} matrix elements from V_{2N} and V_{3N} for the use in the ring diagram calculations. Similar to the half-on-shell T-matrix in the usual Lippmann-Schwinger equation $T(k',k,k^2) = V_{2N}(k',k) + P\int_0^\infty q^2 dq V_{2N}(k',q)\frac{1}{k^2-q^2} \times T(q,k,k^2)$, the effective V_{low-k} interaction is calculated from a T-matrix equivalence requirement.

$$T_{low-k}(p',p,p^2) = V_{low-k}(p',p) + P\int_0^\Lambda q^2 dq V_{low-k}(p',q)\frac{1}{p^2-q^2} \times T_{low-k}(q,p,p^2),$$

with $T(p',p,p^2) = T_{low-k}(p',p,p^2)$; $(p',p) \leq \Lambda$,for V_{2N} and V_{3N}. In the above equations Λ denotes a momentum space cut-off (such as $\Lambda \simeq 2.0 fm^{-1}$), and the symbol $P\int$ the principal-value integration. It was found that under this process, using different realistic potentials would lead to almost the same results in fitting NN phase shifts and deuteron properties. The Lee-Suzuki iteration method [6] has been employed in the calulation of V_{low-k}.

With these ring diagram summed to all orders, the ground-state energy shift from V is given as [2]

$\Delta E_0 = \int_0^1 d\lambda \sum_m \sum_{ijkl\in P} Y_m(ij,\lambda) Y_m^*(kl,\lambda) \times \langle ij|V|kl\rangle$, where (i,j,k,l) are each a shell-model s.p. wave function, and P denotes a chosen shell-model space composed of a set of hole (h) and particle (p) orbits. For example, for ^{16}O we take P as composed of the three h orbits $(0s_{1/2}, 0p_{3/2}, 0p_{1/2})$ and the seven p ones $(0d_{5/2}, ...1p_{1/2})$. The amplitudes Y above are calculated from an RPA-type equation,

$$\sum_{ef}[(\epsilon_i+\epsilon_j)\delta_{ij,ef} + \lambda(1-n_i-n_j)\langle ij|V|ef\rangle] \times Y_m(ef,\lambda) = \omega_m(\lambda) Y_m(ij,\lambda);$$

where $(i,j,e,f) \in P$,and λ a strength parameter, to be integrated from 0 to 1.

The occupation factors are $n_a = 1$ for $a = h$, and = 0 otherwise. Thus the amplitudes $Y_m(ij)$ has only either hh (i=h, j=h') or pp (i=p, j=p') components. The transition amplitudes Y in the equation can be classified into two types, one dominated by hh and the other by pp components. We include only the former, denoted by Y_m, for the calculation of the all-order sum of the $pphh$ ring diagrams.

We use HF s.p. spectrum ϵ_j in the above RPA equation, $\epsilon_j = \langle j|K_{sp}|j\rangle + \sum_h \langle jh|V|jh\rangle$where K_{sp} denotes the s.p. kinetic energy operator. Note that j and h are each oscillator s.p. wave function.

The parameters c_D and c_E in the one-pion exchange and contact terms of V_{3N} are taken from [5] where binding energies of $A = 3$ nuclei were fitted. To calculate the V_{low-k} matrix for V_{2N} and V_{3N} , we have used the Bertsch formula $\hbar\omega = 45.0A^{-1/3} - 25.0A^{-2/3}$ for the nuclear wave functions. The nucleon densities arising from the contact term of V_{3N} for the nuclei considered are chosen as those approximately at the RMS radii from the experimental charge density profiles[7] of the nuclei. The RMS radii for ^{16}O, and ^{40}Ca are 2.7013, and 3.4764 fm[8] respectively. In this way, we set

the densities around the RMS radii to be $0.6\rho_0$ for both ^{16}O and ^{40}Ca, with ρ_0 the nucleon density in nuclear matter. We have also performed theoretical calculations using harmonic oscillator wave functions and obtained similar results.

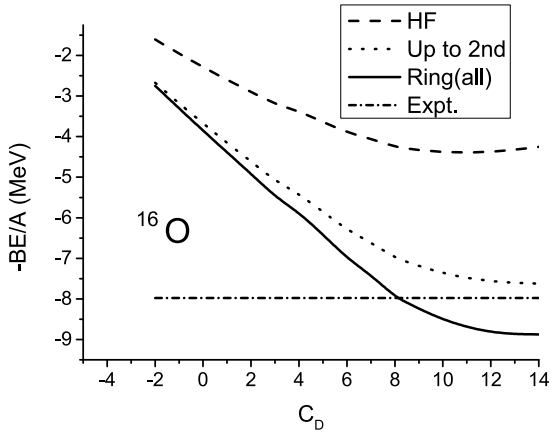

Figure 2. Dependence of $-BE/A$ of ^{16}O on the parameter c_D of V_{3N}.

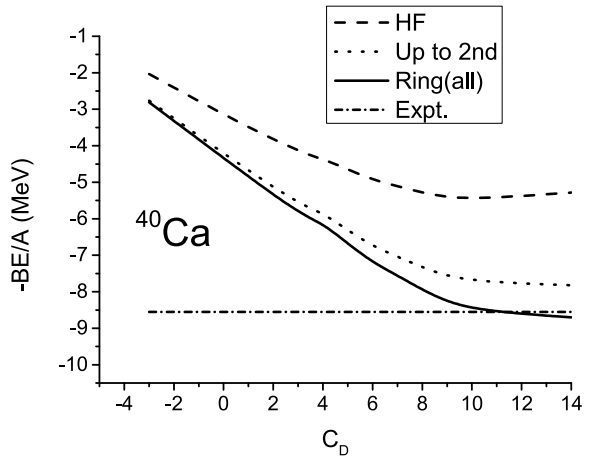

Figure 3. Dependence of $-BE/A$ of ^{40}Ca on the parameter c_D of V_{3N}.

Shown in Figs. 2-3 are the dependence of ground state energies per nucleon (or -BE/A) for ^{16}O and ^{40}Ca on the 3N force constant c_D appearing in V_{3N}. In these figures, results from the first order ring diagram (denoted as "HF"), up to the second order one(denoted as "Up to 2nd"), and all order ring diagrams (denoted as "Ring(all)") are all calculated with V_{3N} included. Experimental data[9] are displayed for comparison. We can see from the figures, although the contribution from diagrams up to the second order one improves quite significantly comparing to that from the first order one alone,

contribution from higher order diagrams is needed to fill the discrepancy so that the experimental binding energy can be obtained. Another feature worth of mentioning is that for both nuclei, the ring diagram results all meet the experimental data at c_D=8.5 and its corresponding c_E from [5].

Also shown in Table 1, our results from V_{2N} + V_{3N} with parameter c_D= 8.5 and its corresponding c_E from [5] at densities ρ/ρ_0= 0.6 for both ^{16}O and ^{40}Ca fit the experimental data [9] quite well. In the Table we also examine the importance of V_{3N} to the nuclear binding energies for both nuclei that we considered. As expected, the binding energies obtained from V_{2N} alone are too weak. The deviation between results with and without V_{3N} gets wider when all ring diagrams are included.

Table 1. -BE/A (in MeV) of ^{16}O and ^{40}Ca, with the same notations as those in Figs.2-3, and c_D = 8.5 for both nuclei.

		ρ/ρ_0	HF	up to 2nd	Ring(all)	Expt
^{16}O	V_{2N}	–	-3.76	-5.17	-5.28	
	V_{2N}+V_{3N}	0.6	-4.30	-7.09	-8.09	-7.976
^{40}Ca	V_{2N}	–	-4.19	-5.89	-6.24	
	V_{2N}+V_{3N}	0.6	-5.37	-7.48	-8.14	-8.551

In summary, we have applied the ring diagram method to calculate binding energy of ^{16}O and ^{40}Ca by adding an in-medium three-nucleon potential V_{3N} to the chiral N^3LO two-nucleon potential V_{2N}. The ground state energy per nucleon so obtained fits the experimental data quite well for each nucleus considered when V_{3N} is added in and all orders of ring diagrams are included. Contributions from ring diagrams with orders higher than 2 can not be ignored. As expected, binding energies obtained with V_{2N} alone are too weak. Our study demonstrates the importance of three-body force in filling in the discrepancy of nuclear binding energies calculated by including only two-body force as compared to the experimental measurements. We believe that the three-nucleon force is also important in other properties of nuclear systems. We are working on this line and will report the results in other publications in the near future.

References

[1] E. Epelbaum, Prog. Part. Nucl. Phys. **57**, 654 (2006); J. W. Holt, N. Kaiser, W. Weise, PRC81, 024002 (2010).

[2] H. Q. Song, S. D. Yang and T. T. S. Kuo, Nucl. Phys. **A462**, 491 (1987).

[3] Yiharn Tzeng, T. T. S. Kuo, Chin. J. Phys. (Taipei) **25**, 326 (1987); Yiharn Tzeng, T. T. S. Kuo, Nucl. Phys. **A485**, 85 (1988).

[4] S. K. Bogner, T. T. S. Kuo and L. Coraggio, Nucl. Phys. **A684**, (2001) 432; S.K. Bogner, T. T. S. Kuo, L. Coraggio A. Covello, and N. Itaco, Phys. Rev. C **65**, 051301(R) (2002); S. K. Bogner, T. T. S. Kuo, and A. Schwenk, Phys. Rep. **386**, 1 (2003).

[5] P. Navrátil, V. G. Gueorguiev, J. P. Vary, W. E. Ormand, A. Nogga, PRL **99**, 042501 (2007).

[6] S. Y. Lee and K. Suzuki, Phys. Lett. **B91** , 173 (1980); K. Suzuki and S. Y. Lee, Prog. Theor. Phys. **64** , 2091(1980).

[7] H. de Vries, C.W. de Jager, and C. de Vries, At. Data Nucl. data Tables **36**, 495 (1987).

[8] I. Angeli, K. P. Marinova, Atomic and Nucl. Data Tables **99**, 69 (2013).

[9] B. Pfeiffer, K. Venkataramaniaih, U. Czok, C. Scheidenberger, Atomic and Nucl. Data Tables **100**, 403-535 (2014); also see Nuclear data from Brookhaven National Laboratory, http://www.nndc.bnl.gov/chart/